ELSEVIER

European Journal of Mechanics B/Fluids 21 (2002) 325–340

EUROPEAN JOURNAL OF MECHANICS B/FLUIDS

Receptivity of a flat plate boundary layer to a free stream axial vortex

Andrey V. Boiko [1]

DLR-Institut für Strömungsmechanik, Bunsenstrasse 10, Göttingen, Germany

Received 5 August 2000; accepted 4 September 2001

Abstract

A single free stream axial vortex of controlled strength and position was used to investigate a vortical receptivity of Blasius boundary layer. Excited boundary-layer disturbances were dominated by streamwise velocity perturbations, that grew downstream essentially linearly with the streamwise coordinate. It was shown that the disturbance characteristics are in agreement with data of previous experiments performed under natural and control conditions concerning the 'by-pass' transition initiated at high free stream disturbance levels. It was proved that the role of the leading edge in the receptivity process and disturbance growth under consideration is not dominant.

Keywords: Receptivity; By-pass transition; Blasius boundary layer; Axial vortex

1. Introduction

It was first recognized more then 50 years ago by Schubauer and Skramsted [1] that wind tunnel free stream disturbances can significantly affect processes in a boundary layer transition zone and make the translation of experimental results obtained there to free-flight conditions a non-trivial problem. An incomplete knowledge concerning the process of interaction of free stream vorticity with boundary layers led the scientific community to the empirical rule of testing the results in several different experimental facilities (see, e.g., [2]). Such an approach is quite time and cost-consuming, being naturally ineffective. Such a background (as well as obvious turbo-machinery applications when free stream turbulence is an imprescriptible participant of the boundary layer development around a blade) stipulates a long-standing interest of the researchers to the problem.

The so-called receptivity phenomenon arises when one tries to provide a reasoning for the origin of turbulence in virtually any open near-wall flow. Turbulence in such a convectively unstable flow is usually a result of a development of some disturbances which appear and start to grow far upstream of the onset of the final transition. Such behaviour is the reason to denote the flows as 'noise amplifiers' in contrast to 'noise generators' governed by non-linear bifurcations [3]. As a consequence, the primary question in the course of receptivity investigation is a search, selection, and experimental as well as theoretical modelling of those mechanisms which are most responsible for the formation of the near-wall disturbance field followed by the transition to turbulence in a particular flow.

The external vortical disturbances in the form of localised quasi-stationary flow modulations or free-stream turbulence (FST) are of those which most frequently contribute to the boundary-layer receptivity [4,5]. Meanwhile, for an effective excitation of a boundary layer disturbance, the vortical forcing must have both the same frequency and comparable spatial scales. From this point of view two types of phenomena are usually distinguished inside the boundary layer: the generation of travelling modes with characteristics of local linear instability and the generation of quasi-stationary longitudinal (vortical) structures or 'streaks',

E-mail address: boiko@itam.nsc.ru (A.V. Boiko).

[1] Current address: ITAM, Novosibirsk 630090, Russia.

0997-7546/02/$ – see front matter
PII: S0997-7546(01)01174-8

which characteristics seems are usually determined by the external vortical disturbances [6,7] both of which can be responsible for the transition to turbulence [8].

The experiments described below were carried out with intention to consider the formation and development of the streak excited in the Blasius boundary layer by a free stream vortex generator similar to that used previously by Bertolotti and Kendall [9].

1.1. Flat plate boundary-layer receptivity to free stream disturbances

Because of the viscous nature of the linear instability of the flow about a flat plate (so-called Tollmien–Schlichting or TS-instability), a localised mechanism of wavelength reduction of the free-stream disturbances which are governed by inviscid dynamics is important. In particular, the effective transformation or 'scattering' of the free-stream disturbances to TS-waves occurs preferably alongside sudden changes of the base flow, e.g., over the leading edge, separation region, suction slits, etc. Since plane 2D TS-waves become unstable first, mostly 2D receptivity mechanisms have been considered experimentally in the past for some test 2D problems (see, e.g., [4,5,10]).

However, both the impossibility of the 2D free stream vortical field to penetrate significantly deep into a 2D boundary layer to interact with the shear flow inhomogenity and the locality of the interaction region make the receptivity relatively weak [10]. This is in contrast to 3D free-stream disturbances which can cause a growth of the streaks. The streaks which received their name due to visualisation patterns produced by the flow structures, are quasi-stationary 3D deformations of the laminar boundary layer which grow downstream by amplitude and length. Their appearance is usually attributed to the so called 'lift-up' effect, i.e. an inviscid redistribution of streamwise momentum by small velocity perturbations in the direction normal to the shear [11,12]. It is noteworthy assumed that the 3D inviscid disturbances already have the scales comparable with the streaks and penetrate deeply into the boundary layer, i.e. the mechanism of the wave-scale reduction is not necessary or is of less significance, so one can expect a quite effective distributive forcing of the streaks along the whole region of the boundary-layer development.

The experimentally observed disturbance motion produced by the streaks is sometimes referred to as a 'Klebanoff mode', due to early observations of Klebanoff with coauthors [13,14], who found steady and low-frequency spanwise periodic modulations of the streamwise velocity component in the Blasius boundary layer produced by a residual inhomogenity raised by wind tunnel damping screens. Later the mean and fluctuating characteristics of the flat plate boundary layer subject to the 3D free-stream disturbances in the form of nearly isotropic FST has been studied extensively, e.g., in experiments [7,15,16], and led to a selection of a series of phenomenological characteristics inherent for the 'streak' motion inside boundary layers.

Flow visualisations like that in [17] show that the streaks start to develop at the leading edge of the plate. However, the idea of the distributed receptivity mechanism is supported by a series of experiments, see [18] and references therein. In particular, it was shown that localised disturbances introduced by means of a short-time blowing through a narrow pipe placed in a free stream in front of a model can initiate the development of transient boundary-layer structures at the leading edge, which are very similar to what we known about the FST induced streaks. However, the observed continuous decay of the locally introduced disturbance amplitude in all tested cases is in contrast to the continuous downstream growth of the streamwise disturbance observed in the presence of FST.

Similar conclusions on the inability of localised receptivity mechanisms to describe the observed streak growth in the Blasius boundary layer were given by Bertolotti [19], based on a consideration of both the experiments [20] and the asymptotic theory [21]. Kendall [20] measured no difference in the disturbance amplitude for two different values of the leading-edge bluntness, i.e. it was independent of the flow structure in that region. It was also argued that the disturbance growth based on the local receptivity mechanism of the asymptotic theoretical model [21] occurs at the flow velocities and wind tunnel conditions of reference experiments [6,7,20,22] only at unnaturally large distances from the leading edge. As a consequence, Bertolotti [19] excluded the leading-edge effect from his receptivity theory. He linked Klebanoff modes to FST by incorporating non-parallel effects and studied the distributed response of the Blasius boundary layer to 2D and 3D vortical modes satisfying the linearised Navier–Stokes equations in the free stream, which were used to represent some key features of low-level turbulence at small frequencies. It appeared that the computed results presented in [9,19] agree basically with measurements of the boundary-layer response to free-stream turbulence, but still the role of the leading edge was not definitely clarified.

1.2. Experimental simulation of the receptivity process

To be able to apply modern synergetic experimental-computational approaches in a receptivity research, a particular receptivity mechanism has to be considered in a 'purified' environment to reveal underlying physical background. It can be achieved through a choice of simplified flow geometries and eliminating possible 'side effects', e.g., by noise reduction, and subjecting the flow to controlled influence of different factors, e.g., excitation of controllable disturbances.

Nishioka and Morkovin [4] discussed some of the basic requirements to describe a particular receptivity mechanisms under investigation. In context of the present work these are: application of an appropriate forcing; quantitative characterisation of the

flow and forcing fields along the outer edge of the boundary layer and leading edge; local information on the fluctuations in the boundary layer in the region under consideration.

In a recent experiment [9], with the main goal to compare the boundary-layer response with a theoretical receptivity model, it seems that a reasonable way to introduce some controlled 'representative' vortical disturbances from the free stream into a boundary layer was found. A model vortex in the experiment originated at the tip of a micro-wing positioned above a flat plate being in front of the leading edge. By varying the wing's angle of attack and the free-stream velocity the vortex strength can be controlled. Such an approach gives a fundamental possibility to investigate the development of the stationary disturbances in detail and in a quiet environment independently of travelling modes. The successful comparison between the Bertolotti's theory and the Kendall's measurements of the response of the boundary-layer [9] indicates that in such a way the receptivity of the flow to quasi-stationary disturbances could be modelled. The same approach with some modifications discussed below was used in present study.

2. Experimental procedure

2.1. Experimental set-up and measurement technique

Because of the uncontrollable effect of free-stream disturbances on transition experiments, one of the aims of the study was to minimise the disturbance intensity as much as possible. To achieve it, the investigations were done in a low-turbulence wind tunnel of DLR, Göttingen (TUG), see its drawing at www.sm.go.dlr.de/sm-sm_info/TRTinfo. The TUG is a wooden contoured wind tunnel with a closed test section and open diffuser located in a closed room. The turbulence level is reduced by means of a set of turbulence damping screens and 16 : 1 contraction nozzle. The test section is 6.25 m long, 0.3 m wide and 1.5 m high. The operation velocities of the wind tunnel are in the range 4 to 45 m/s. In the region of current measurements, the turbulence level appeared to be independent on the downstream coordinate and velocity, being characterised by certain anisotropy: $u' = 0.19$, $v' = 0.07$, and $w' = 0.06\%$ of U_0, so that $Tu = \sqrt{(u'^2 + v'^2 + w'^2)/3} \approx 0.12\%$ of U_0.

The flat plate model was the same as in the experiments of [23,24] being 1500 mm wide, 1175 mm long, and 40 mm thick. The model consists of a main plexiglas body polished to 0.2 μm roughness, a trailing edge flap and a leading edge. The leading edge is elliptical with the axis-ratio 6 : 1 to eliminate possible leading edge separation. The trailing edge flap was used to adjust the pressure distribution at the leading edge as close to zero as possible. The model was vertically installed along the test section axis. The large model span prevents disturbances from wall junctions to contribute the measurements along the centerline in the spanwise range of about 200 mm up to the distance about 1 m from the leading edge.

The coordinate system used was the following: the x axis directed from the leading edge along the plate chord, z is parallel to the edge with $z = 0$ being 40 mm aside from the plate centerline, and y is normal to the wall and zero at it. Measurements of the streamwise velocity component were carried out in the central part of the plate in the range of $\Delta z = 80$ mm and $x = 217-480$ mm at $U_0 = 5.9$ and 7.8 m/s above the plate.

The sketch of the experimental setup is given in Fig. 1. The vortex in the experiments originated at the tip of a micro-wing. A 0.6 mm thick and 5 mm wide NACA FXL V152 K25 profile with 0.3 mm rounded edges and sides was used. It was glued to a long round holder of 8 mm diameter. To minimise possible end effects and the effect of the holder, the micro-wing had 80 mm

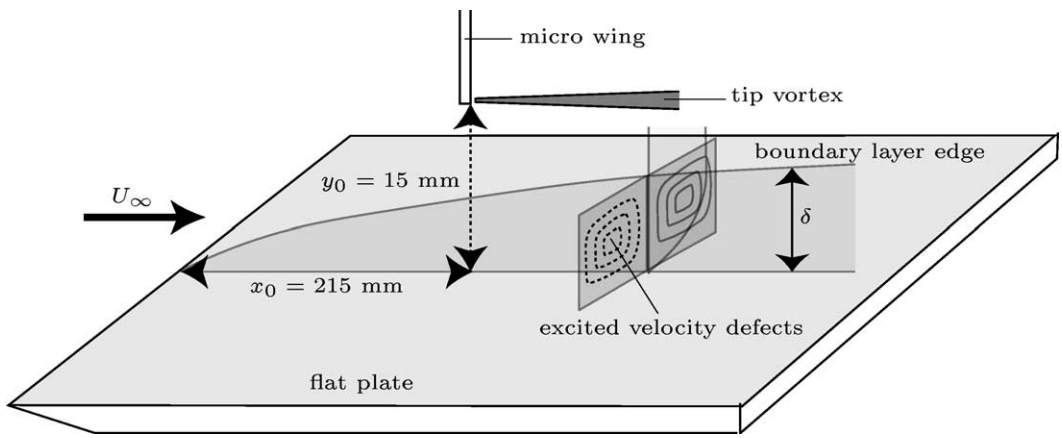

Fig. 1. Sketch of the experimental setup.

span. The vortex strength was controlled by varying the micro-wing angle of attack and the ambient velocity. The micro-wing tip was located at $y_0 = 15$ mm from the wall and $x_0 = 215$ mm from the leading edge.

Different mean and fluctuating velocity components were obtained by means of standard constant-temperature DISA hot-wire anemometers using standard DISA V- and X-arranged hot wire probes. The boundary-layer measurements were done with V-arrangement. Such probes neglect the normal-to-the-wall velocity component but allow one measurements close to the wall. The free-stream measurements were performed with X-probes. The probe axis was aligned with the free-stream direction so that, to measure both crosswise velocity components, the wires can be rotated manually by 90° along the axis, holding the probe spatial location.

Signals from two independent hot-wire anemometers were digitised by a 12-digit A/D converter. Analogue signal conditioners consisted of differential amplifiers with voltage offset were used to subtract fixed constant voltages from the bridges and to improve the system dynamic range and resolution of sampled signal. The wires were made of gold plated tungsten of 5 μm diameter with a sensitive length of about 1 mm, operating at 80% overheat, and calibrated against a Prandtl tube in the free stream. The samples were linearised and processed with a personal computer in MATLAB 5.3 environment. Since the free stream velocities of the experiment were rather small, the air heating due to friction losses, which contributes mostly to changes of temperature in the flow at higher velocities, did not occur and consequently the overheat correction with time was not applied.

Multi-axis traversing mechanisms controlled by a personal computer were used for the probe positioning. The probes could be moved automatically in x, y, and z directions as well as manually positioned at different angles in the (xz)-plane, the last being significant for V- and X-wire calibrations. The traversing mechanisms allowed one to perform spatial measurements with relative accuracy 12.5 μm in x and z directions and 7.5 μm in y direction. Due to some technical restrictions, the absolute accuracy of setting the origin of z-axis after shifting to a new x-position over the flat plate or after a probe calibration procedure is approximately ± 1 mm. Mean and disturbance velocity profiles along y were measured with spacing 0.2–0.3 mm in near-wall region of stronger wall-normal velocity gradient to get better resolution and 0.3–0.5 mm closer to outer border of the boundary layer.

There is a problem with the reconstruction of velocity components at double-wire measurements inside of both the spanwise modulated boundary layer and the free stream tip vortex due to the presence of streamwise velocity gradients along the transverse directions. Since the probe wires are located in different points along a transverse coordinate, the difference of the streamwise velocities between them is interpreted by the linearisation routine as a fictitious transverse velocity for both the X- and V-like probes. The idea of the correction method consists in collection of voltages from the anemometers with the step Δz (or Δy) equal to the distance between the wire centres followed by their spatial synchronisation using the data in a staggered order. It is also possible to choose another step Δz (or Δy), in which case it is necessary to carry out at first an interpolation of the data with the step equal to the distance between the wire centres.

The necessity to use the measurements performed at different time leads, generally, to some restrictions on the determination of disturbance values. Namely, it is possible to reconstruct only correct values of stationary and phase-coherent periodic velocity components, for the last purpose a trigger must be used to start the data acquisition at every point. Since only stationary data are presented, the restriction does not affect results of the present study. A more detailed description of this method and its error estimations can be found, e.g., in [25].

2.2. Calibration

Instead of a standard King's law formula for a single wire calibration, a modified function was used during the measurements:

$$U = k_1\left(E^2 - E_0^2\right)^{1/n} + k_2(E - E_0)^{1/2},$$

where E is an anemometer voltage, U is a corresponding streamwise velocity, E_0 is the anemometer voltage at zero velocity, and k_1, k_2, n are adjustable constants to be determined for the best least square fit to the calibration data. The value of $1/n$ was usually close to 2. The second semi-empirical term accounts for the contribution from free convection at low velocities and makes it possible to correct hot-wire measurements close to the wall (see [26] and reference therein for details). Meanwhile, it should be noted, that results obtained with the help of the above formula and the standard King's law at the smallest velocities measured in the present experiment of about 0.9 m/s differ by less then 1%. That could be a rough upper estimation of the absolute accuracy of the streamwise velocity measurements close to the wall under these experimental conditions.

Two-velocity component measurements in the present study required more involved calibration and linearisation procedures. In practice, the use of the well known and originated from clear physical background analytical cosine law and its modifications [27] to build calibration dependencies lead to a quite pronounced error in the determination of spanwise velocity components *at small flow velocities* (less then approximately 2 m/s) due to a relatively large contribution of a free convection around the heated wires and a heat transfer to the wall. Another approach based on the application of direct look-up (interpolation) tables, first developed probably in [28] was used with some modifications. In particular, an extrapolation of the

Table 1
Integral flat plate boundary-layer characteristics (Blasius values are in brackets)

U_0, m/s	Δx, mm	δ^*, mm	H	Re_{δ^*}
	2	1.21 (1.31)	2.56 (2.59)	476
5.9	40	1.44 (1.42)	2.58 (2.59)	566
	130	1.63 (1.64)	2.54 (2.59)	641
	265	1.99 (1.93)	2.67 (2.59)	782
	2	1.09 (1.15)	2.72 (2.59)	567
7.8	40	1.28 (1.24)	2.62 (2.59)	666
	130	1.43 (1.43)	2.79 (2.59)	744
	265	1.69 (1.68)	2.62 (2.59)	879

calibration to the range of small velocities to use the two-wire measurements close to the wall was additionally applied by means of the above described modified King's law formula.

The calibration was done at 7–10 velocities (from 0.8 to 9 m/s) and 21 angles (from –25 to 25° with equal step), at every velocity. There is a fundamental restriction on the range of angles allowed for hot-wire probes, due to a multi-variance of the calibration data at angels $\Phi \gtrsim 30°$, when a correct velocity reconstruction becomes impossible. It limits the measurements to a crosswise–streamwise velocity rate less then approximately 0.5, which was never reached during the study. To minimise possible error at low velocities due to a drift of wire characteristics with time, the duration of the measurements between two successive calibrations was usually less then 8 hours.

2.3. Description of the base flows. Estimation of the probe distance to the wall from the experimental data

Since the flat plate was aligned at zero angle of attack, the velocity distribution inside the most part of the boundary layer must be very close to the Blasius one. It is well known (see, e.g., [29]) that the boundary layers along an ideal flat plate must obey certain theoretical laws, i.e. it is quite easy to check the quality of the flows from the point of view of their theoretical description.

Specifically, the Blasius boundary layer is characterised by the displacement thickness $\delta^* = 1.72\sqrt{xv/U_0}$ and a constant shape factor $H = \delta^*/\vartheta = 2.59$, where ϑ is a momentum-loss thickness. Trying to take into account the region of the boundary-layer formation close to the leading edge, a modified formula for the calculation of δ^* is widely used with $x \mapsto x + x_v$, where x_v is a 'virtual' origin of the plate called to correct the theoretical values. It was found that a small value of $x_v = 14$ mm provides the best, but rather minor correction for both test velocities $U_0 = 5.9$ and 7.8 m/s. The corresponding experimental and calculated data are given in Table 1. The most significant difference occurs at the front-most point in both cases. Downstream, the theoretical and experimental values of δ^* differ by less then approximately 3%, i.e. the agreement is quite good. The difference at the front-most point may probably be explained by an effect of pressure gradient about the thick leading edge, as in the other flat plate measurements (see, e.g., [30]). The correspondence between values of H is not so accurate. Its calculation involves both the momentum-loss thickness ϑ, also taken from experimental data subject to an error, and the division, the operation which is additive for the errors in numerator and denominator.

Since the usual strategy during measurements is to exclude possible damages of hot-wire sensors if they are occasionally dragged along the wall when traversing, the measurements were carried out starting with an approximately 0.3 mm offset. At the same time an accurate knowledge of the distance is significant for characterisation of mean and fluctuating boundary-layer parameters.

The wire offset to the wall was estimated by a global fit of experimentally measured velocity profiles in the laminar boundary layers to the theoretical Blasius profile using the least-square technique with the offset as the unknown to be found. A cubic interpolation of tabulated theoretical values in experimental points was used. The upper limit of absolute accuracy of the fitting procedure is estimated as ± 0.02 mm. It was done by a comparison of the results with those of a local linear extrapolation of the experimental profiles close to the wall. The result of application of this procedure for the boundary layer is shown in Fig. 6.

3. Results

3.1. General observations

To prove that the manufactured micro-wing arrangement is able to produce a laminar tip vortex, a simple visualisation by means of hydrogen bubble technique was performed in the DLR small water tunnel (see www.sm.go.dlr.de/sm-sm_info/

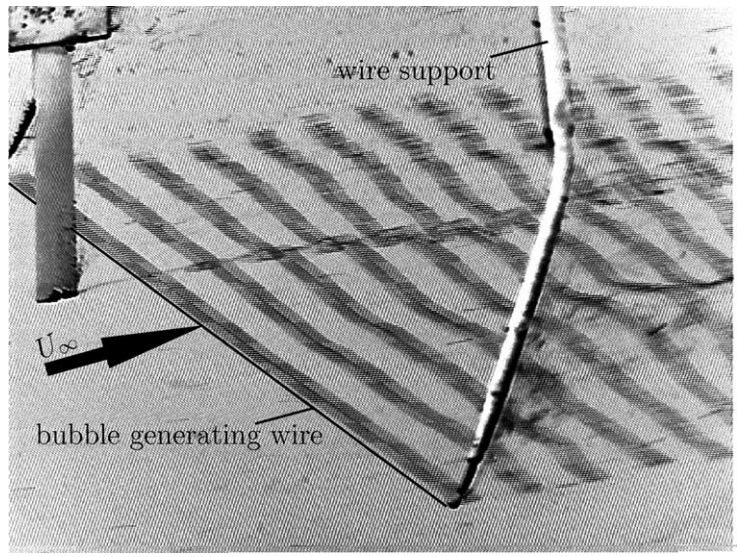

Fig. 2. Micro-wing tip vortex hydrogen bubble visualisation in a water tunnel at $Re = 0.25 \cdot 10^4$.

TRTinfo for its detail description) at a Reynolds number based on the micro-wing chord $Re = 0.25 \cdot 10^4$. This value is very close to the maximum $Re = 0.26 \cdot 10^4$ used in the main wind tunnel experiments. A thin bubble-generating wire was located downstream of the micro-wing in a position made it possible to observe the vortical motion emanating from the wing. The data were recorded by a commercial video camera so, to capture a range of the tip vortex development to approximately 75–80 mm downstream of the micro-wing. Some shoots were transformed with the help of a frame grabber into a computer readable form and processed there. A typical frame is presented in Fig. 2. Despite a more detailed analysis was not performed, a uniform rotational motion accompanied by presence of streamwise velocity defect in the vortex center was observed, when the micro-wing was positioned at a small angle of attack. At larger angles of attack the motion became highly distorted, showing quite abrupt transition of the laminar regime to the turbulent one. In general, the motion appears to be visually similar to that investigated in more detail in [31] behind a large straight wing at higher Reynolds numbers. The most significant difference in the present case consists in the absence of vortex pair interaction, since the other micro-wing edge did not produce the second tip vortex.

3.2. Development of the free stream tip vortex above the flat plate

To provide initial conditions for the interaction between the vortex and the boundary layer, the tip vortex mean axial and circumferential velocity components were measured in several (yz)-planes downstream of the micro-wing above the flat plate. To obtain the streamwise velocity defect $\Delta U = U - U_0$ and the circumferential velocity Ω, the streamwise U and both transverse velocities V and W were measured by an X-wire probe rotated manually by 90° around its axis. Then Ω was reconstructed using the formula $\Omega = \sqrt{V^2 + W^2}$. The data of ΔU and Ω were 'unwrapped' in polar coordinate system with its origin located in the vortex center. Neighbouring points were used to estimate the value of data 'scattering' that roughly correspond to a random error of the data measurements. The obtained mean velocities and error bars based on the data standard deviations in ± 0.15 mm ranges are presented against the radial coordinate r in Fig. 3 for $\Delta x = 40, 130$, and 265 mm downstream of the micro-wing. The data show a slow downstream decay of the vortex at both velocities accompanied by a little expansion of its core that is in accordance with previous observations [31]. The corresponding maximum streamwise velocity defect ΔU, maximum circumferential velocity Ω, and the radius of the vortex core R (the distance from the vortex axis to the location of Ω maximum) are given in Table 2.

The characteristic feature of the motion is the appearance of both the streamwise and the circumferential velocity defects. It is considered that one of the reasons of quantitative disagreement in measured and calculated boundary-layer response to the tip vortex forcing in [9] is an oversimplified vortex model used to describe the tip vortex free-stream behaviour. In particular, the wing tip vortex was modelled in [9] as a Hamel–Oseen vortex. However, the model neglects the induced streamwise velocity defect, which is quite large in the current experiment, in experiments [31], and probably in experiment [9]. To overcome this discrepancy, Bertolotti (private communication) suggested to use a more advanced Batchelor model [32] describing a similarity

Table 2
Mean tip vortex characteristics above the flat plate downstream of the micro-wing

U_0, m/s	Δx, mm	R, mm	$\Delta U/U_0$	Ω/U_0
	40	1.33	–0.143	0.115
5.9	130	2.00	–0.063	0.069
	265	2.33	–0.048	0.050
	40	1.33	–0.153	0.132
7.8	130	1.66	–0.093	0.097
	265	2.00	–0.059	0.075

solution of the flow in the tip vortex far downstream of the wing. In terms of similarity coordinate $\eta = U_0(r/2)^2/(\nu x)$, the streamwise velocity defect produced by the vortex is expressed as

$$\Delta U = \frac{\gamma_0^2 P(\eta) - U_0^2 S\mathrm{e}^{-\eta}}{8\nu x},$$

where $\gamma_0 = \Gamma_0/2\pi$, Γ_0 denotes circulation at the vortex origin. S is a constant with the dimension of area and the second term accounts for any initial velocity defect which may be independent from circulation. The term P is given by the formula

$$P(\eta) = \mathrm{e}^{-\eta}\big[\log(\eta/Re_x) + \mathrm{Ei}(\eta) - 0.807\big] + 2\mathrm{Ei}(\eta) - 2\mathrm{Ei}(2\eta),$$

where $\mathrm{Ei}(\eta) = \int_\eta^0 \mathrm{e}^{-\xi}/\xi\,\mathrm{d}\xi$ is the exponential integral function. An asymptotic solution for the circumferential velocity component Ω far away downstream of the wing tip is found as $\Omega = \gamma_0(1 - \mathrm{e}^{-\eta})/r$. According to measurements [31], such self-similar behaviour of the tip vortex occurs at distances from the wing of $x/L \gtrapprox 10$. In the present experiment only the position closest to the wing at the chord length $L = 5$ mm is close to this semi-empirical limit, while all other positions satisfy this criterion. From the other side, the Batchelor's analysis is correct at large x, if the condition is satisfied: $\|\Delta U/U_0\|_{r=0} \ll 1$. It seems that this is also true in all the cases considered with the possible exception at the front-most position measured $\Delta x = 40$ mm, see Table 2.

The above formulae were applied to fit all sets of the experimental data obtained by means of multi-variable least-square technique, see Fig. 3. To improve the fit, a 'virtual' vortex origin was used, so that $x \mapsto x + x_\mathrm{v}$. The data used for the best vortex approximation at $U_0 = 5.9$ m/s: $\gamma_0 = 1.8 \cdot 10^{-4}$ m^2/s, $S = 5.46 \cdot 10^{-2}$ mm^2, $x_\mathrm{v} = 140$ mm, and 7.8 m/s: $\gamma_0 = 2.1 \cdot 10^{-4}$ m^2/s, $S = 3.44 \cdot 10^{-2}$ mm^2, $x_\mathrm{v} = 120$ mm. As can be seen, they quite accurately predict the vortex development, and although this was not used later in the present study, it may be helpful for future theoretical flow modelling.

Knowing the circulation and applying the Prandtl wing theory, one can derive, that for a free wing, the self-induced motion of the pair of the tip vortices along z-axis is $W = 4\gamma_0/(\pi b)$, where b is the wing span [31]. In the case under consideration, the other side of the wing did not produce a tip vortex, since it was glued to the holder. Meanwhile, in this case one can expect a certain induced motion, due to appearance of an effective dipole system in the presence of the wall. The rough estimation gives for both test cases the upper limit of the motion close to $W/U_0 = 1.2 \times 10^{-2}$, that corresponds to shift of only about $\Delta z \approx 3.2$ mm over the measurement region $\Delta x = 2$–265 mm. In fact, no reliably resolved vortex shift was captured in present measurements.

3.3. Flat plate boundary-layer measurements

An observed large response in the streamwise component was in contrast with the spanwise velocity component in the boundary layer, which appeared to be very small for reliable measurements. Therefore, only data based on the streamwise velocity measurements are presented below.

Isolines of the velocity defect measured at several x locations downstream of the micro-wing are given in Fig. 4. As can be seen, the defects experience continuous growth at both velocities, while the disturbance spanwise structure remains the same, showing one velocity maximum and one minimum with spacing between them, in fact, independent of the downstream coordinate and equal to 20 ± 2 mm for both test cases. The boundary layer remains laminar, without a presence of detectable TS-waves, although the measurements were done in the region of their instability which starts at $Re_{\delta^*} \approx 520$, that corresponds to $x \approx 215$ and 160 mm for $U_0 = 5.9$ and 7.8 m/s, respectively, i.e. background disturbances usually causing them were negligible.

Since these measurements were carried out separately from the free-stream measurements described above, the direct comparison of the boundary-layer response and tip vortex relative location is impossible. Nevertheless, it was tried to check the presence of the induced spanwise motion in the boundary layer, since sometimes the streaks are interpreted as stationary streamwise vortices. However, because both the traversing mechanism did not preserve exactly the same z when moving along x and the manual positioning of the probe after every day calibration was accurate to $\Delta z \pm 1$ mm, separate checks for both test

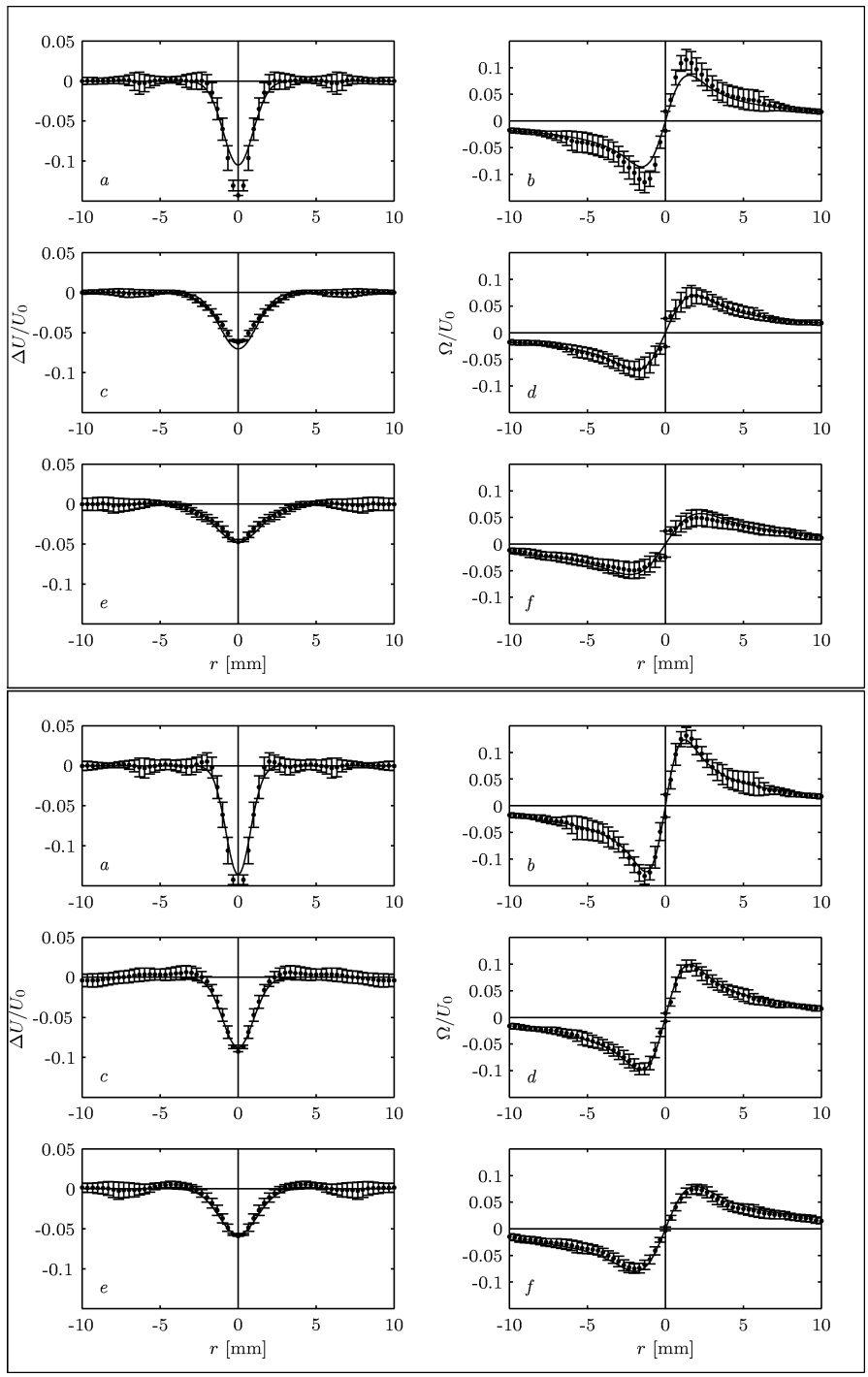

Fig. 3. Tip vortex development in free stream at $\Delta x = 40$, 130, and 265 mm (top to down). $U_0 = 5.9$ m/s (upper part) and 7.8 m/s (lower part). *a*, *c*, *e* – streamwise velocity defect; *b*, *d*, *f* – circumferential velocity. Points – measured mean values; bars – error estimations; solid lines – data approximation by means of the Batchelor model.

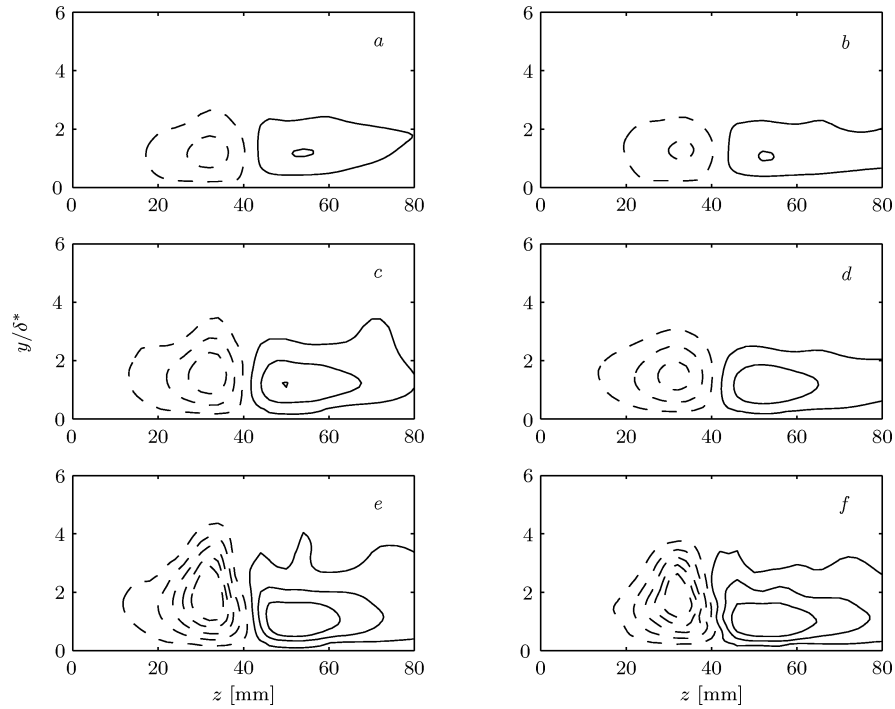

Fig. 4. Velocity defects induced in the flat plate boundary layer by the free stream tip vortex at $\Delta x = 40$, 130, 265 mm. Sets: *a, c, e* and *b, d, f* at $U_0 = 5.9$ and 7.8 m/s, respectively. Solid lines – excesses, dash lines – defects. Equidistant isolines from –0.290 to 0.140.

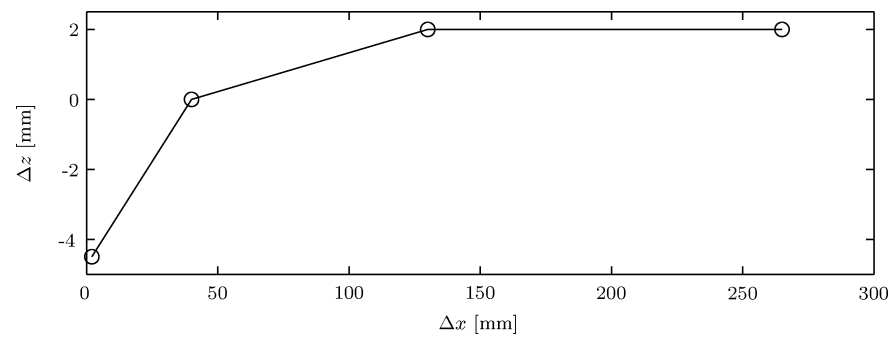

Fig. 5. Relative downstream shift of the inflection point $\partial^2 U/\partial z^2 = 0$ at the position of disturbance maximum $y/\delta^* = 1.3$ for $U_0 = 5.9$ and 7.8 m/s.

velocities were impossible. Meanwhile, for each streamwise coordinate x, the measurements at both test velocities were carried out directly one after the other. Consequently, the difference between the spanwise motion at these velocities can be detected, e.g., by comparison of the spanwise locations of a certain characteristic point of the induced disturbance.

For such relative estimations, the inflection point $\partial^2 U/\partial z^2 = 0$ is a good choice if the general disturbance structure is preserved at both velocities as in the case under consideration. The location of the inflection point was estimated by cubic spline interpolation of the experimental data, followed by analytic double differentiation of the resulting spline functions. In fact, a certain relative shift Δz was observed as presented in Fig. 5. It can be seen, that the shift is monotonic and is of the same order as the expected for the tip vortex, see Section 3.2. Taking into account that the measurements at both test velocities were done consequently escaping calibration and repositioning procedures, the mentioned absolute inaccuracy in traversing can hardly explain the *relative* difference between the shifts, i.e. the detected tendency does indicate a presence of a certain vorticity in the induced motion. However, the vorticity is very small, since the spanwise velocity in the region of the disturbance localisation was not detectable by the direct V-wire measurements as described earlier.

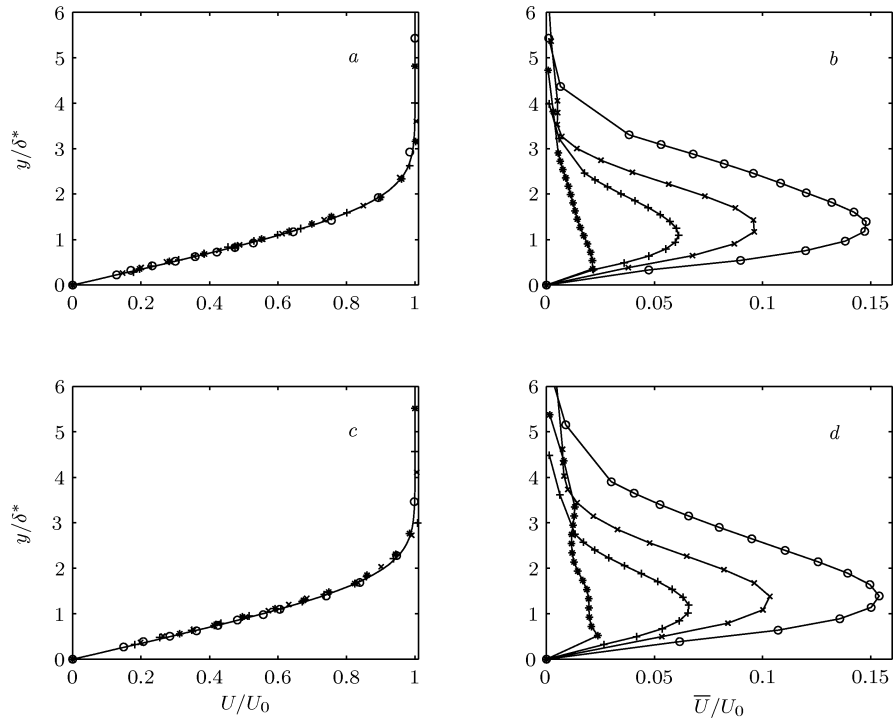

Fig. 6. Mean and disturbance boundary-layer characteristics at Δx: $*$ – 2; $+$ – 40; $\times$ – 130; $\circ$ – 265 mm. *a*, *c* – experimental laminar profiles at $U_0 = 5.9$ and 7.8 m/s (points), theoretical Blasius profile (solid lines); *b*, *d* – standard deviations of the boundary-layer profiles due to the presence of stationary disturbance.

For a better understanding of the nature of the velocity defect growth in the boundary layer, where stationary disturbances are stable according to local parallel linear stability theory, a further analysis was undertaken. Averaged mean velocity profiles, the theoretical Blasius profile, and the corresponding distribution of the standard deviation of the mean velocity defect

$$\overline{U}(y) = \sqrt{\int_{z_{\min}}^{z_{\max}} \Delta U(y,z)^2 \,\mathrm{d}z/\Delta z},$$

approximated by a cubic spline interpolation of the experimental data over the region of the velocity-defect localisation $\Delta z = z_{\max} - z_{\min} = 80$ mm, are shown in Fig. 6 for certain distances downstream of the micro-wing. As can be seen, the presence of the vortices does not significantly affect the mean velocity distribution, although $\overline{U}(y)$ reaches about 15% of U_0 at the end of the measurement region. Except at the points closest to the micro-wing, the disturbance maximum is located at nearly the same coordinate scaled with the boundary layer displacement thickness $y/\delta^* \approx 1.3$ and their shapes are, in fact, close to self-similar. The same conclusion was done previously in [16,33] concerning the shape of the naturally occurring Klebanoff mode at a high FST level.

The remarkable feature of the quasi-stationary disturbances excited in flat plate boundary layer under the effect of homogeneous FST to hold H close to the laminar value up to their amplitudes of 10% of U_0 was documented in [30]. The corresponding variations of δ^*, ϑ and H found in the present experiment are given in Fig. 7. In contrast to quite large variations of the first two parameters, the mean and individual values of the shape factor in the region of vortex localisation are also close to the laminar value $H = 2.59$, being in accordance with the average behaviour of mean flow profiles in Fig. 6.

The simplest way to estimate the growth of the disturbances is to consider their magnitude as the difference between the maximum disturbance excess and defect. It was done, e.g., in [9], when the boundary-layer streak was excited by a tip vortex from a micro-wing located *in front of* the flat plate. It was found there both experimentally and theoretically, that the magnitude grows essentially linearly with x for the case of stationary disturbances, the slope of the growth being smaller with the micro-wing tip distance to the wall. Results of current measurements, when the micro-wing was located *above* the flat plate are shown in Fig. 8 for both velocities. Moving the micro-wing further from the wall means that a more peripheral part of the tip vortex (and/or associated pressure disturbance) interacts with the boundary layer. In the present case, the measurements were done at the fixed tip distance $y_0 = 15$ mm, but at different free-stream velocities, corresponding to different local Reynolds

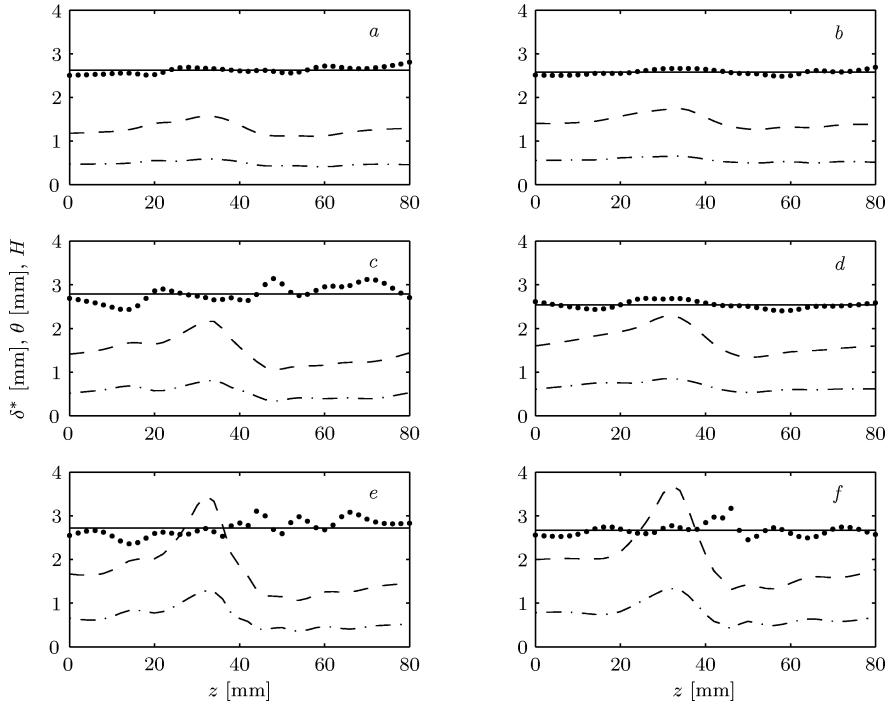

Fig. 7. Integral boundary-layer characteristics across the disturbed boundary layer: dash lines – δ^*; dash-dotted lines – ϑ; points – H; solid lines – averaged H. $U_0 = 5.9$ (left) and 7.8 (right) m/s. Δx: *a, b* – 40; *c, d* – 130; *e, f* – 265 mm.

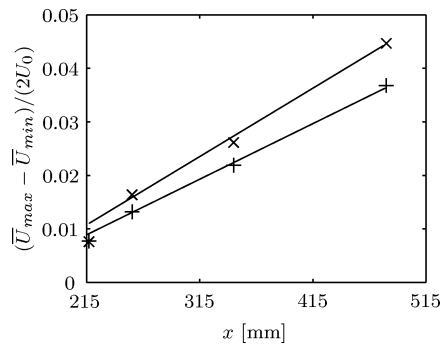

Fig. 8. The effect of the vortex strength on the boundary-layer response, U_0: + – 5.9; × – 7.8 m/s.

numbers (and also boundary layer thicknesses) and different tip-vortex vorticities (Fig. 3). As can be seen in both test cases, the disturbance growth is linear with x and the curve slope is smaller for the case of the tip vortex with more peripheral part interacting with the boundary layer. Combined with the data [9] these results prove, that the leading edge plays no dominant role in this mechanism of the stationary streak amplification for the Blasius boundary layer, the growth being essentially linear with x at least under present experimental conditions.

At the same time, the growth of the vortex magnitude is not the best measure, because it can be subject to a pronounced error due to inaccuracy in determination of the velocity defect and excess at the discrete spatial measurements. From this point of view, an amplitude $\overline{U}(y)$, based on standard deviation of the mean velocity defect which calculation includes an integration is a better choice. The downstream growth of maximum value of $\overline{U}(y)$ is shown in Fig. 9 for both test velocities. It is seen, that the disturbance grows linearly between the last three points, when the disturbance maximum is stabilised at $y/\delta^* \approx 1.3$. The dependence of the growth on the range of integration was checked by cutting out side regions of the disturbance from calculation of $\overline{U}(y)$. As can be seen, in modifying the integration range inside so wide limits the growth is still linear, indicating *posteriori* that the chosen measurement window is appropriate for the following quantitative data analysis.

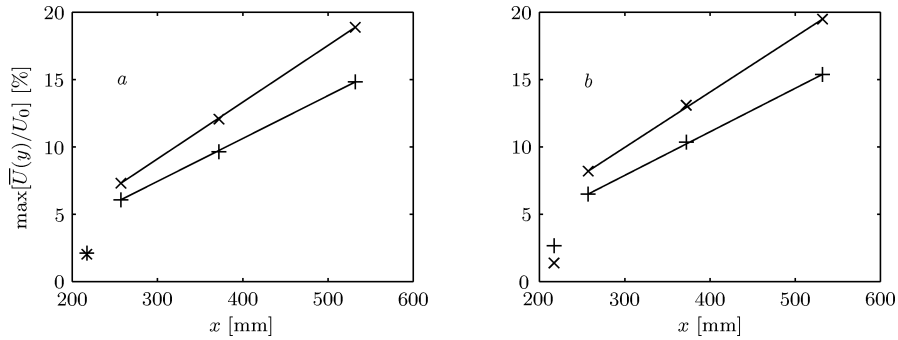

Fig. 9. Disturbance growth along its maximum: + – half range; × – full range, U_0: *a* – 5.9; *b* – 7.8 m/s.

The velocity defect at a fixed x can be considered spectrally as a localised wave packet consisting of independent stationary waves with different spanwise wave numbers β and zero real part of streamwise wave number α_r as well as frequency ω. Since the packet is not periodic, instead of a discrete Fourier analysis, one has to use an integral Fourier transformation to investigate its spanwise structure:

$$\Delta U(y,\beta) = \frac{1}{2\pi}\int_{z_{\min}}^{z_{\max}} \Delta U(y,z)\mathrm{e}^{-\mathrm{i}\beta z}\,\mathrm{d}z,$$

with the integration range limited to the measurement region of $\Delta z = 80$ mm and supposing that $\Delta U(y,z) \approx 0$ beyond it. Special tests concerning the integration range, based on its artificial extension by zero padding and small variation of the edge conditions, showed that the wave number spectrum is reliably resolved at β from approximately 0.02 to 0.40 mm^{-1}.

The result of this transformation is shown in Fig. 10. Already 2 mm downstream of the micro-wing, disturbances are localised inside the boundary layer and centered around $\beta = 0.06$–0.12 mm^{-1}. This tendency is further reinforced downstream, where disturbance maximum is concentrated at fixed $\beta \approx 0.08$ mm^{-1} and $y/\delta^* \approx 1.3$ mm for both velocities. This results are in accordance with above discussed independence of the distance between the disturbance excess and defect in Fig. 4. This definitely indicates that in the frame of the current experimental conditions the scale of the excited structure depends on neither the changes in tip vortex intensity nor changes of the boundary-layer thickness in the region of the streak generation and propagation ($\delta^* = 1.09$–1.99). The last is also in accordance with measurements [34] at $Tu \approx 1.5\%$, where stationary velocity modulations maintained their spanwise scale during the downstream propagation. Similarly, in a model experiment [18] localised isolated free-stream disturbance ('puff') excited boundary-layer streaks of its own conservative scale.

Based on the data shown in Fig. 10, the disturbance growth integrated across the boundary layer up to the boundary-layer edge δ^* can be calculated: $\overline{U}(\beta) = [\int_0^\delta \Delta U(y,\beta)^2\,\mathrm{d}y/\delta^*]^{1/2}$. The normalisation by δ^* is used to take into account the observed self-similarity of the disturbances in coordinates y/δ^*. It is known that in a non-parallel boundary layer, the disturbance growth can depend on the measure chosen. To check it in the present case, two commonly accepted measures were selected: the integral growth and the growth along the disturbance maximum at $y/\delta^* = 1.3$. The results are shown in Fig. 11 for the same coordinates as in Fig. 10. It is seen that both methods give very close shapes of disturbance intensity distribution, conforming self-similarity of the excited disturbances and indicating insignificance of the flow non-parallelism at this stage on the streak development.

As for the case of the disturbance growth over the range of resolved β, Fig. 9, the growth at individual β is linear with x, that is illustrated in Fig. 12. As can be seen, the growth in the considered range of β is, in fact, also independent on the spanwise wave number.

Amplitude functions $\widehat{\overline{U}}(y)$ for this series of β are shown in Fig. 13. It demonstrates a self-similarity of the amplitude distribution of the excited 'modes'. As can be seen, all of them have a single maximum about $y/\delta^* \approx 1.30$. Such a self-similarity was observed at all other x, except at the front-most one. Moreover, the observed self-similarity of the 'modes' is consistent with the recent analysis [35] of optimal transient disturbances in the Blasius boundary layer. Dimensionalised for the conditions of the present experiment, data of [35] show virtually independent shape of longitudinal velocity oscillations induced by the optimal oscillations at least in the range $\Delta\beta \approx 0.12$–0.86 mm^{-1}.

The remarkable similarity of the disturbance shapes found in different experiments and obviously far from optimal as well as of the shapes obtained with the help of different theoretical models has been mentioned repeatedly in literature [7,9,36] and discussed extensively by Luchini [35]. Klebanoff's observations that the streamwise velocity component of the naturally observed streaks at a high FST resembles quasi-stationary modulations of the Blasius mean velocity profile, when the local boundary-layer thickness experiences small changes referred to as the 'breathing' [22]. Such a 2D breathing may be caused by, e.g., small amplitude oscillations in time of both the stagnation line at the leading edge and the free-stream velocity. The

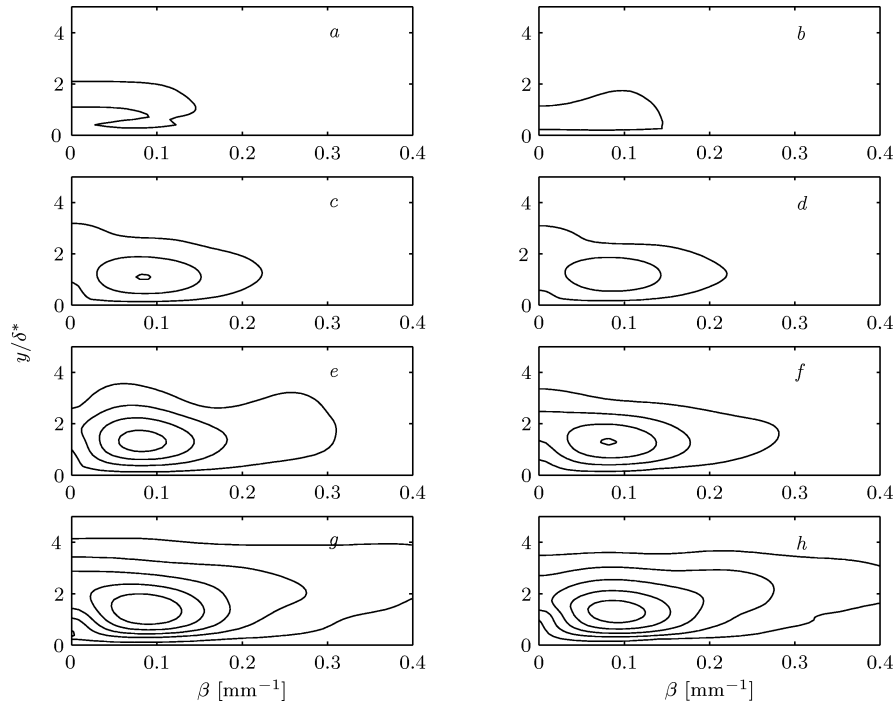

Fig. 10. Spectral distribution of ΔU: *a*, *c*, *e*, *g* and *b*, *d*, *f*, *h* at $U_0 = 5.9$ and 7.8 m/s. $\Delta x = 2$, 40, 130, 265 mm (top to down). Equidistant isolines from 0.1 to 1.1.

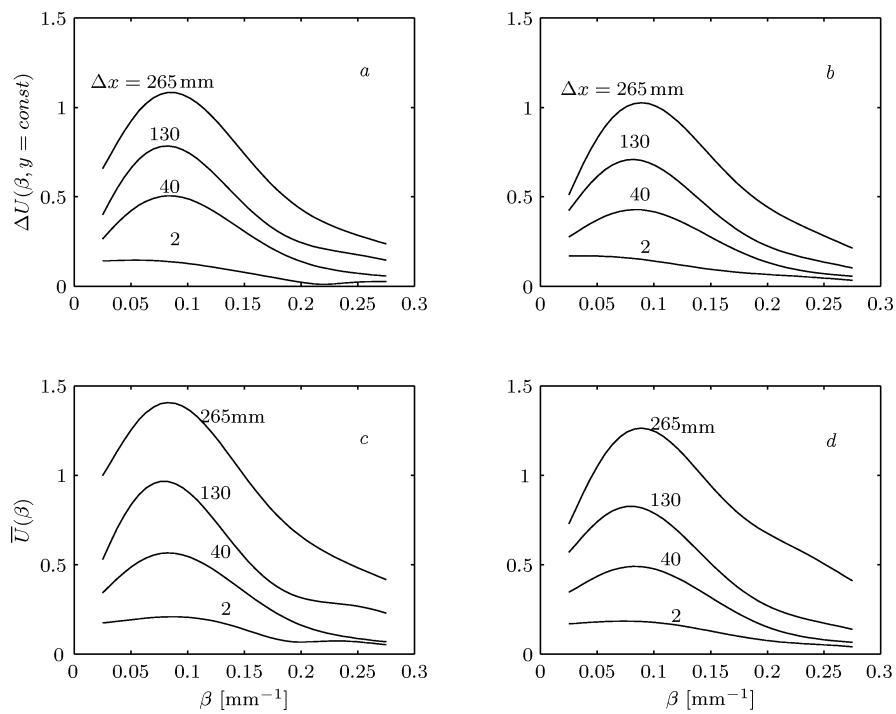

Fig. 11. Spectral disturbance growth along $y/\delta^* = 1.3$ (top) and integrated over the range $y/\delta^* = 0$ to 5 (bottom), U_0: *a*, *c* – 5.9; *b*, *d* – 7.8 m/s.

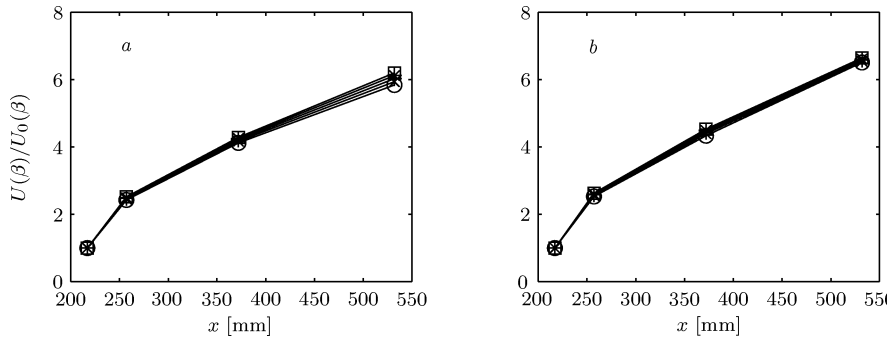

Fig. 12. Disturbance growth integrated across the boundary layer for individual β: $\circ - 0.050$; $\times - 0.075$; $+ - 0.100$; $* - 0.125$; $\square - 0.150$ mm^{-1}. U_0: $a - 5.9$; $b - 7.8$ m/s.

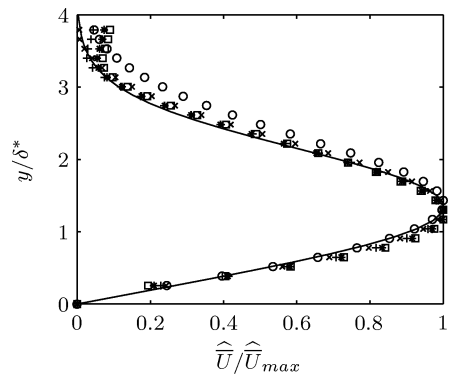

Fig. 13. Disturbance velocity profiles at $U_0 = 5.9$ m/s, $\Delta x = 130$ mm for individual β: $\circ$ – 0.050; $\times$ – 0.075; $+$ – 0.100; $*$ – 0.125; $\square - 0.150$ mm^{-1}. Solid line – the normalised shape of the disturbance produced by quasi-stationary variations of the boundary-layer thickness.

shape of this small amplitude breathing has an analytical expression to be $y\partial U/\partial y$ [37]. Normalised by its maximum, it is shown in Fig. 13 by the solid line. As can be seen, it almost perfectly follows the amplitude shapes of individual 3D stationary modes found in the present study. The feature, that the shapes of the stationary modes can be obtained from such a simple 2D quasi-stationary treatment is quite remarkable and led Luchini to the conjecture that the velocity shape of the breathing mode is a kind of attractor for the most initial conditions.

However, such localised quasi-stationary 2D treatment of the breathing origin hardly can either explain the observed disturbance amplitude or their growth, since the Blasius boundary-layer thickness depends on the square root of the free-stream velocity and distance from the leading edge and small changes in these values are felt less and less by the boundary layer further downstream. This means, that the breathing excited in such a way always decays with x, the possible exception being the region very close to the leading edge, where the Blasius boundary-layer approximation is invalid.

4. Conclusion

The responses of a flat-plate boundary-layer to free stream axial vortex was considered. It was found that the generation of a single streak occurs. This streak has the same phenomenological characteristics as those which appeared in the boundary layer under the effect of a high FST levels. In particular, it has the only amplitude maximum which location in normal-to-the-wall direction scales with the boundary-layer thickness at $y/\delta^* = 1.3$; the dimensional scale of the streak in spanwise direction is preserved; its amplitude growth is essentially linear with x-coordinate; whereas its magnitude reaches several percent of free-stream velocity, the streak causes only a moderate effect on integral boundary-layer characteristics. The streak vorticity (or equivalently, its spanwise and wall-normal velocities are very small). A comparison with study [9] shows that the leading edge can play no dominant role in the receptivity process and disturbance growth.

The results can be used in theoretical receptivity models as test data due to simplicity of description of the axial vortex characteristics and the performed detailed analysis of the boundary layer response.

Two natural extensions of the results are the deepening of the knowledge on the vortical receptivity in this and other realistic flow models as well as application of the technique to excite quasi-stationary disturbances. In fact, the receptivity due to the quasi-stationary free-stream axial vortices for both swept wing and flat plate cases was studied recently by the author with the help of the slowly oscillating micro-wing. The data are currently in the processing stage.

Acknowledgements

The work was financially supported by the Alexander von Humboldt Foundation and the German Aerospace Center (DLR), Institute for Fluid Mechanics, Göttingen, Germany. The experimental facilities were provided by the DLR. The author express a lot of thanks to Drs H. Bippes (unfortunately deceased), F. Bertolotti, C. Abegg and Prof. U. Dallmann from the Institute for their personal support and valuable discussions as well as to the technical stuff of the Institute: Mr D. Baumgarten, H. Denecke, D. Hübner, and H. Mattner as well as to the director of the Institute Prof. G. Meyer and to Prof. V.V. Kozlov from ITAM, Novosibirsk, Russia, whose joint idea of this visit was so fruitful.

References

[1] G.B. Schubauer, H.K. Skramsted, Laminar-boundary layer oscillations and transition on a flat plate, NACA TN 909 (1948).
[2] H. Bippes, Basic experiments on transition in three-dimensional boundary layers dominated by crossflow instability, Prog. Aerospace Sci. 35 (1999) 363–412.
[3] P. Huerre, P.A. Monkewitz, Absolute and convective instabilities in free shear layers, J. Fluid Mech. 159 (1985) 151–168.
[4] M. Nishioka, M.V. Morkovin, Boundary-layer receptivity to unsteady pressure gradients: experiments and overview, J. Fluid Mech. 171 (1986) 219–261.
[5] V.V. Kozlov, O.S. Ryzhov, Receptivity of boundary layers: asymptotic theory and experiment, Proc. Roy. Soc. London A 429 (1990) 341–373.
[6] J.M. Kendall, Boundary layer receptivity to freestream turbulence, AIAA Paper 90-1504, 1990.
[7] K.J.A. Westin, A.V. Boiko, K.G.B. Klingmann, V.V. Kozlov, P.H. Alfredsson, Experiments in a boundary layer subjected to free stream turbulence. Part 1. Boundary layer structure and receptivity, J. Fluid Mech. 281 (1994) 193–218.
[8] A.V. Boiko, K.J.A. Westin, K.G.B. Klingmann, V.V. Kozlov, P.H. Alfredsson, Experiments in a boundary layer subjected to free stream turbulence. Part 2. The role of TS-waves in the transition process, J. Fluid Mech. 281 (1994) 219–245.
[9] F.P. Bertolotti, J.M. Kendall, Response of the boundary layer to controlled free-stream vortices of axial form, AIAA Paper 97-2018, 1997.
[10] Y.S. Kachanov, Physical mechanisms of laminar-boundary-layer transition, Annu. Rev. Fluid Mech. 26 (1994) 411–482.
[11] L.S. Hultgren, L.H. Gustavsson, Algebraic growth of disturbances in a laminar boundary layer, Phys. Fluids 24 (6) (1981) 1000.
[12] G.R. Grek, V.V. Kozlov, M.P. Ramazanov, Three types of disturbances from the point source in the boundary layer, in: V.V. Kozlov (Ed.), Laminar-Turbulent Transition, IUTAM Symposium, Springer-Verlag, Novosibirsk, 1985, pp. 267–272.
[13] P.S. Klebanoff, K.D. Tidstrom, Evolution of amplified waves leading to transition in a boundary layer with zero pressure gradient, NACA TN D-195 (1959).
[14] P.S. Klebanoff, K.D. Tidstrom, L.M. Sargent, The three-dimensional nature of boundary-layer instability, J. Fluid Mech. 12 (1962) 1–34.
[15] D. Arnal, J.C. Juillen, Contribution érimentale à l'étude de la réceptivité d'une couche limite laminaire, à la turbulence de l'écoulement général, CERT RT 1/5018 AYD, ONERA, Juin 1978.
[16] V.S. Kosorygin, N.P. Polyakov, Laminar boundary layers in turbulent flows, in: D. Arnal, R. Michel (Eds.), Laminar-Turbulent Transition, IUTAM Symposium, Springer-Verlag, Toulouse, 1990, pp. 573–578.
[17] P.H. Alfredsson, A.A. Bakchinov, V.V. Kozlov, M. Matsubara, Laminar-turbulent transition at a high level of a free stream turbulence, in: P.W. Duck, P. Hall (Eds.), Nonlinear Instability and Transition in Three-Dimensional Boundary Layers, Fluid Mechanics and its Application, Kluwer Academic Publishers, Manchester, 1996, pp. 423–436.
[18] K.J.A. Westin, A.A. Bakchinov, V.V. Kozlov, P.H. Alfredsson, Experiments on localised disturbances in a flat plate boundary layer. Part 1: The receptivity and evolution of a localised free stream disturbance, Eur. J. Mech. B/Fluids 17 (6) (1998) 823–846.
[19] F.P. Bertolotti, Response of the Blasius boundary layer to free-strem vorticity, Phys. Fluids 9 (8) (1997) 2286–2299.
[20] J.M. Kendall, Studies on laminar boundary layer receptivity to freestream turbulence near a leading edge, in: D.C. Reda, H.L. Reed, R. Kobayashi (Eds.), Boundary Layer Stability and Transition to Turbulence, Vol. FED-114, ASME, 1991, pp. 23–30.
[21] M.E. Goldstein, S.J. Leib, Cowley S.J., Distortion of a flat-plate boundary layer by free-stream vorticity normal to the plate, J. Fluid Mech. 237 (1992) 231–260.
[22] J.M. Kendall, Experimental study of disturbances produced in a pre-transitional laminar boundary layer by weak free stream turbulence, AIAA Paper 85-1695, 1985.
[23] M. Fischer, Untersuchung künstlich angeregter Instabilitäten in einer zweidimensionalen Grenzschichtströmung mit Hilfe der Particle Image Velocimetry, DLR-FB 93-58, 1993.
[24] M. Wiegel, Experimentelle Untersuchung von kontrolliert angeregten dreidimensionalen Wellen in einer Blasius-Grenzschicht, in: Reihe 7: Strömungstechnik, no. 312, VDI Verlag GmbH, Düsseldorf, 1997.

[25] H. Deyhle, Einfluß der äußeren Strömungsbedingungen auf den Transitionsprozeß einer dreidimensionalen Grenzschich, in: Reihe 7: Strömungstechnik, no. 226, VDI Verlag GmbH, Düsseldorf, 1993.
[26] A.V. Johansson, P.H. Alfredsson, On the structure of turbulent channel flow, J. Fluid Mech. 122 (1982) 295–314.
[27] H.H. Bruun, Hot-wire Anemometry: Principles and Signal Analysis, Oxford University Press, 1995.
[28] W.W. Willmarth, T.J. Bogar, Survey and new measurements of turbulent structures near wall, Phys. Fluids 20 (1977) S9–S21.
[29] H. Schlichting, K. Gersten, Boundary Layer Theory, 8th ed., Springer-Verlag, 2000.
[30] K.G.B. Klingmann, A.V. Boiko, K.J.A. Westin, V.V. Kozlov, P.H. Alfredsson, Experiments on the stability of Tollmien–Schlichting waves, Eur. J. Mech. B/Fluids 12 (4) (1993) 493–514.
[31] H. Bippes, Experimente zur Entwicklung der freien Wirbel hinter einem Rechteckflügel, Acta Mech. 26 (1977) 223–245.
[32] G.K. Batchelor, Axial flow in trailing line vortices, J. Fluid Mech. 20 (1964) 645–658.
[33] V.S. Kosorygin, N.F. Polyakov, T.T. Suprun, E.Y. Epik, Development of disturbances in laminar boundary layer of a plate at high free stream turbulence level, in: Levchenko V.Y. (Ed.), Instability of Sub- and Supersonic Flows, RAS. Sib. Branch. Inst. Theoret. Applied Mech., Novosibirsk, 1982, pp. 85–92 (in Russian).
[34] M. Matsubara, A.A. Bakchinov, P.H. Alfredsson, Global scaling of disturbance structure in boundary layer transition induced by free stream turbulence, Abstract submitted to the IUTAM Symposium on Laminar-Turbulent Transition, 1999.
[35] P. Luchini, Reynolds-number-independent instability of the boundary layer over a flat surface: optimal perturbations, J. Fluid Mech. 404 (2000) 289–309.
[36] S. Berlin, D.S. Henningson, A nonlinear mechanism for receptivity of free-stream disturbances, Phys. Fluids 11 (12) (1999) 3749–3760.
[37] P.A. Libly, H. Fox, Some perturbation solutions in laminar boundary-layer theory, J. Fluid Mech. 17 (1964) 433–449.